Mineralogical Magazine, October 2006, Vol. 70(5), pp. 545–564

Petrology and geodynamic significance of deerite-bearing metaquartzites from the Escambray Massif, Cuba

C. GREVEL[1, †], W. V. MARESCH[1,*], K.-P. STANEK[2], F. GRAFE[1,‡] AND S. HOERNES[3]

[1] Institut für Geologie, Mineralogie und Geophysik, Ruhr-Universität Bochum, D-44780 Bochum, Germany
[2] Institut für Geologie, TU Bergakademie Freiberg, Bernhard-von-Cotta-Str. 2, D-09596 Freiberg, Germany
[3] Mineralogisch-Petrographisches Institut und Museum, Poppelsdorfer Schloss, D-53115 Bonn, Germany

ABSTRACT

Deerite, a typical mineral of Fe-rich metacherts metamorphosed under blueschist conditions, is not rare, but known occurrences have up to now been restricted mainly to the Tethyan collisional zone and the Western Cordillera of North America. We describe a first occurrence in the high-pressure nappes of the Escambray Massif, Cuba, in the assemblage deerite + Mg-Al-poor riebeckite + magnetite + quartz ± garnet ± phengite ± aegirine. This assemblage typically forms during exhumation and accompanies late, stress-free annealing of the quartz matrix. Mg-Al-poor riebeckite overgrows older, large, oriented crystals of glaucophane, ferroglaucophane and Mg-Al-rich riebeckite ('crossite') during deerite formation. Early-formed hematite was largely replaced by magnetite. Deerite is very close to ideal composition, attaining >99% $Fe^{2+}_{12}Fe^{3+}_{6}Si_{12}O_{40}(OH)_5$, allowing direct application of the experimentally determined *P-T-*f_{O_2} stability field (Lattard and Le Breton, 1994). In combination with oxygen-isotope thermometry on magnetite-quartz, the crystallization conditions of the deerite-bearing assemblage can be constrained to ~470ºC, >15 kbar, and an oxygen fugacity restricted closely to the quartz-fayalite-magnetite buffer ($f_{O_2} \approx 10^{-23}$ bar). Thus, the late-stage *P-T* path of the metacherts mirrors a steep *P-T* gradient of 10ºC/km or less, requiring subduction of this part of the Antillean Island Arc to be still active during exhumation of the Escambray nappes.

KEYWORDS: deerite, high-pressure metamorphsm, metaquartzite, Escambray Massif, Cuba, oxygen-isotope thermometry.

Introduction

ALTHOUGH previously described by Lacroix (1941) and Coleman and Lee (1963), deerite was identified as a new mineral by Agrell *et al*. (1965) from the famous Laytonville quarry, Mendocino County, California. Since then, deerite has been reported from >20 localities in the world (see summaries by Langer *et al*., 1977; Muir Wood, 1979; Lattard and Le Breton, 1994; Deer *et al*., 1997). Nevertheless, these occurrences are very restricted in terms of rock type, metamorphic grade and geodynamic setting. Deerite is known only from blueschist-facies ferruginous metasediments. The presence of deerite requires Fe-rich, relatively Al-poor bulk compositions and geothermal gradients below 10ºC km^{-1} (Lattard and Le Breton, 1994). Geographically, known deerite localities are confined to the Tethyan realm extending from the Western Alps to New Caledonia, the Île de Groix occurrence (Bretagne, France; Dudek and Kienast, 1987), and to the Western Cordillera of North America from California to the State of Washington.

Lattard and Le Breton (1994) have suggested that deerite may actually be much more common than usually assumed, and may have been widely overlooked in the past. Although the structure is based on hybrid single-double silicate chains (Fleet, 1977), i.e. a "loop-branched vierer single-chain" in the systematic terminology of

* E-mail: walter.v.maresch@ruhr-uni-bochum.de
† present address: TÜV Rheinland, Am Grauen Stein, D-51105 Cologne, Germany
‡ present address: IBeWa Consulting, Lessingstraße 46, D-09599 Freiberg, Germany
DOI: 10.1180/0026461067050349

Liebau (1985), deerite forms virtually black, acicular needles with lozenge-shaped cross-sections and good {110} cleavage very reminiscent of amphiboles.

In the present paper, we describe the first occurrence of deerite in the Caribbean area from the Escambray Massif, an isolated mountainous area of metamorphic rocks in Central Cuba. In addition, the composition of this deerite is very close to the ferrous-ferric end-member $Fe^{2+}_{12}Fe^{3+}_{6}[Si_{12}O_{40}](OH)_{10}$, for which Lattard and Le Breton (1994) have provided comprehensive experimental stability data. Thus, the presence of deerite is also an invaluable aid in estimating pressure-temperature conditions of metamorphism for the complex heterogeneous nappe pile represented by the Escambray Massif.

Geological setting

Cuba is located at the northwestern margin of the Caribbean Sea, ~150 km south of Florida (Fig. 1). In geodynamic terms, the geology of Cuba represents a key element in our attempts to understand the complex plate tectonic evolution of the Caribbean area and to clarify contradictory interpretations (e.g. Pindell and Barrett, 1990; Meschede and Frisch, 1998; Iturralde-Vinent, 1994; Kerr *et al*., 1999; Stanek, 2000; Stanek *et al.*, 2000; Giunta *et al*., 2002; Pindell *et al.*, 2005). During the Late Cretaceous and Paleogene the oceanic Great Antillean island arc and its associated subduction-accretion complex collided and merged with the pre-Mesozoic basement of North America (Yucatán and Bahamas platform; Iturralde-Vinent, 1994). The original structure of this Northern Caribbean Suture Zone is well preserved in Cuba, and the suture is clearly evident as the Cuban Main thrust (Fig. 1). In the north and northwest of Cuba, the rocks can be related to the continental margins of the Bahamas Platform and the Yucatan Peninsula, whereas in the south we find rocks of the Cretaceous oceanic island arc and associated ophiolites.

To the rear (south) of this continent-arc collisional suture, and associated with the Cretaceous island arc, tectonic windows expose metamorphic rocks throughout the southern part of the Island of Cuba (Fig. 1). With an exposed area of ~1800 km^2, the Escambray Massif (Fig. 1) is the largest metamorphic complex of the Greater Antilles. The massif forms two morphological

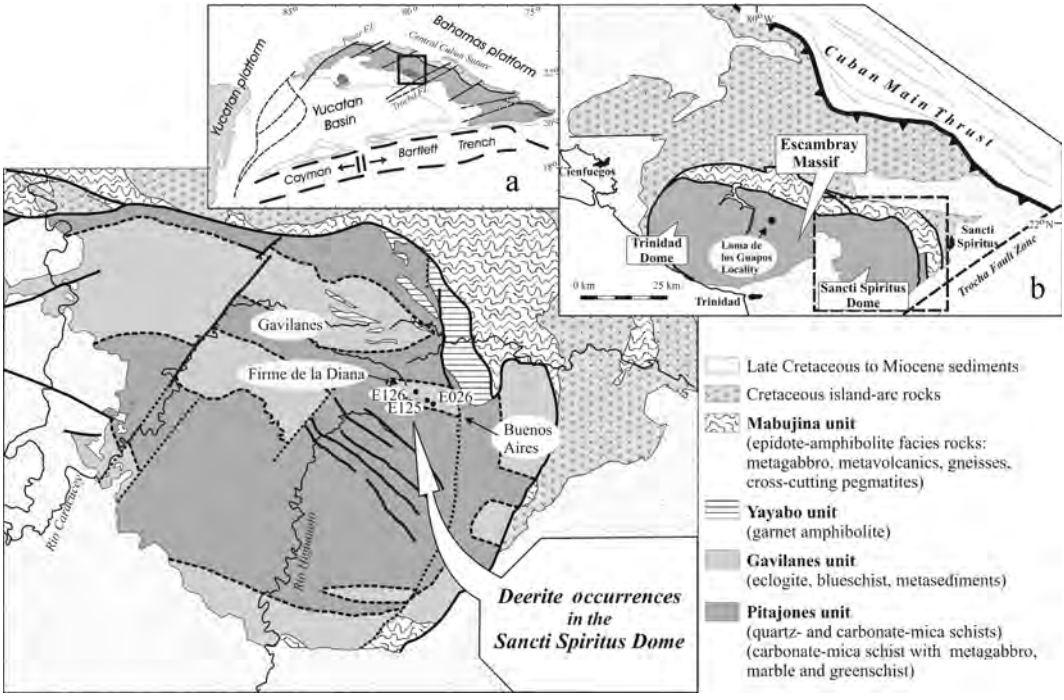

FIG. 1. Geological sketch map of the Escambray Massif indicating localities discussed in text.

domes, the western Trinidad and the eastern Sancti Spiritus dome (Somin and Millán, 1974). Considerable discussion has accompanied attempts to provide a tectono-metamorphic nomenclatural framework for the Escambray Massif, with ideas evolving from early concepts based only on lithological correlation to the recognition that the Massif represents a complex nappe pile (Somin and Millán, 1981; Millán and Somin, 1985*a*,*b*; Millán-Trujillo, 1997; Stanek *et al*., 2000, 2006) Our own coordinated structural, petrological and geochronological work in the Sancti Spiritus dome, beginning in 1992 (e.g. Stanek, 2000; Stanek *et al*., 2000; Grevel, 2000; Grafe, 2001; Stanek *et al*., 2002, 2006) has led us to recognize four major tectono-metamorphic nappes (Fig. 1), which can be discriminated on the basis of their contrasting pressure-time-paths. From bottom to top we distinguish the intermediate- to high-pressure Pitajones, Gavilanes and Yayabo nappes, which are in turn overlain by the low-pressure Mabujina nappe.

The teconically lowermost nappe (Pitajones unit) consists of monotonous carbonate- and quartz-mica schists with abundant boudins of marble, metagabbro and greenschist in its upper part. Maximum preserved equilibration pressures are ~8 kbar (Grevel, 2000). The overlying Gavilanes nappe is a tectonic megabreccia containing quartzite, blueschist, eclogite, amphibolite and serpentinized ultramafic rocks in a general matrix of impure metacarbonates, quartz-mica schists and marbles. Preserved maximum pressures vary from 15–23 kbar (Grevel, 2000; Schneider *et al*., 2004). The Yayabo unit is restricted to the northeastern part of the Sancti Spiritus dome (Fig. 1). Intercalated slivers of this unit have also been reported from the upper parts of the Gavilanes unit (Somin and Millán, 1981). The Yayabo unit comprises fine- to coarse-grained, epidote-bearing garnet-amphibolites. Omphacite is not observed, but barroisitic amphiboles are typical. Maximum pressures of 13–15 kbar are indicated (Grevel, 2000). Low-pressure/high-temperature, amphibolite- to greenschist-facies rocks (metagabbros and metadiorite, foliated plagiogranite, porphyroblastic amphibolites, quarzite) constitute the Mabujina unit, the tectonically highest nappe of the Escambray Massif. The internal structure of this nappe is concordant with the overall structure of the Escambray metamorphic complex, in which the foliation dips gently south on the southern flank and steeply north along the northern rim. Peak *PT* conditions of ~7 kbar at 620–700ºC (Grevel, 2000) support the regional temperature estimates of Somin and Millán (1981). The Mabujina and the Yayabo units were tectonically juxtaposed at conditions of ~4 kbar and 510–540ºC. The contact is now characterized by penetrative ductile shearing with an associated greenschist-facies overprint. We interpret the Mabujina unit as a remnant of the Cretaceous island arc and the Yayabo nappe as a highly deformed and dismembered part of the island arc separating arc sequences in the hanging wall from the footwall subduction-accretion complex of the Gavilanes and Pitajones units (Stanek *et al*., 2002, 2006).

Occurrence and observed mineral assemblages of deerite-bearing metaquartzites

Quartz-rich metasediments occur in a number of localities in both the Trinidad and Sancti Spiritus domes of the Escambray Massif. However, we have found rocks interpretable as metacherts in only two localities. They are found in the Sancti Spiritus dome along the valley trail leading from the village of Buenos Aires to the Firme de la Diana, the 560 m pass providing the SE entrance to the central valley in which the village of Gavilanes is situated (Fig. 1), and at Loma de los Guapos in the Trinidad dome. At Buenos Aires all occurrences are within the Gavilanes nappe. At Loma de los Guapos the lithological relationships are not well exposed. Nevertheless, rock type, metamorphic grade and structure appear to correlate with the Gavilanes nappe of the Sancti Spiritus dome (Millán-Trujillo, 1997; Stanek *et al.*, 2000). Brief reference to additional possible metachert localities are contained in the field descriptions of Somin and Millán (1981) and Stanik *et al.* (1981).

At Buenos Aires very fine-grained white to greyish metaquartzites are intercalated with strongly weathered greenish carbonate and quartz-mica schists in the steep, incized trail directly below the Firme de la Diana pass. The metaquartzites vary from massive to well foliated, depending on the amount of mica present and the preferred orientation of sodic amphibole. A conspicuous feature are mm–cm-thick, alternating dark- and light-coloured layers. Strong boudinage of the light-coloured, quartz-rich layers and superimposed penetrative shearing leads to brecciated rock types and even massive, featureless examples. Needles of blue amphibole up to

TABLE 1. Mineral assemblages observed at the Buenos Aires locality. UTM-coordinates of the sample locations are: E026 (647 255, 242 2442), E124 (645 800, 242 3673) and E125 (646 939, 242 2855). Samples M562 and S149 are splits from the same boulder. Detailed data for samples indicated in bold are given in this paper.

Sample location	E026 (boulder)	E124 (*in situ*)		E125 (boulders)							
Sample no.	**M562/S149**	**G2074**	G2075	**G2077**	**G2079**	G2076	G2078 to G2081	G2080	G2082 to G2085	G2086	G2087
Deerite	X	X		X?							
Blue amphibole	X	X	X	X	X	X	X	X	X	X	X
Magnetite	X	X		X	X						
'Early' hematite*	X			X							
'Late' hematite*	X	X		X	X						
Cr-Spinel		X			X						
Undiff. oxides			X			X	X	X	X	X	X
Quartz	X	X	X	X	X	X	X	X	X	X	X
Garnet		X		X	X						
Epidote									X	X	X
White K-mica				X	X			X			X
Chlorite		X					X		X		
Aegirine					X						
Apatite					X						

* see text for discussion

several cm long are commonly well oriented and define a strong linear fabric. Further southeast towards Buenos Aires, where the valley widens and flattens, fresh metaquartzite occurs strewn in the pastures and vegetable fields as rounded boulders up to several metres in diameter. These rocks present a tough, massive challenge to the hammer. Thin sections of 15 samples were taken from the Buenos Aires locality.

The mineral assemblages observed in the Buenos Aires locality are summarized in Table 1. The macroscopically distinct dark layers can consist of up to 90 vol.% spinel (solid solutions of hercynite, chromite and magnetite) and/or hematite, which alternate with the quartz-rich layers. Deerite was discovered in the two metaquartzites M562 and G2074. Exceedingly small brownish crystallites in the extremely quartz-rich sample G2077 (>94 wt.% SiO_2, Table 2) are probably also deerite, but the crystal size precluded unequivocal identification and analysis. The bulk of the minerals other than quartz tend to be segregated in layers or irregular schlieren. Increasingly penetrative shearing leads to a distinctly planar fabric and thinning of the darker layers until these may consist only of trails of aligned single crystals. Later tempering has led to a polygonal fabric in the quartz matrix and unoriented growth of younger generations of amphibole and mica. Deerite growth is related to this period of static annealing.

Four samples from Buenos Aires were selected for further macro- and microchemical characterization, in particular the two rocks containing unequivocal deerite. Sample M562 represents a large boulder with distinct bluish sheen and linear fabric, whereas G2074 characterizes an integral part of the metasedimentary series of the Gavilanes nappe. In M562, platelets of opaque Fe oxide trace the foliation and unidirectionally oriented coarse, zoned, idiomorphic crystals of blue amphibole accentuate the macroscopically observed linear fabric (Fig. 2). Nevertheless, the quartz matrix is strongly recrystallized with foam structure, and younger generations of very fine-grained blue amphibole and deerite form unoriented needles and sprays of needles throughout (Fig. 3), suggesting late, stress-free annealing at depth. Specimen S149 is from the same block as M562 and was originally taken as a large-volume sample for zircon geochronology.

In sample G2074 the preferred orientation of the older generation of larger amphiboles is less distinct. The conchoidal schlieren of mafic minerals accentuate the basic augen-like fabric of the polygonal quartz matrix. No zonation of the amphibole is evident optically. As in M562, smaller needles of unoriented blue amphibole and deerite are scattered throughout the quartz matrix. Garnet is almost completely replaced by chlorite. Two additional samples were studied mainly for comparative purposes. G2077 is a very

TABLE 2. Bulk composition of Buenos Aires metacherts. Major elements in wt.%, trace elements in ppm.

Sample	M562	G2074	G2077	G2079		M562	G2074	G2077	G2079
SiO_2	87.66	84.04	94.22	82.07	Ba	0	0	0	0
TiO_2	0.01	0.04	0.04	0	Co	347	209	38	197
Al_2O_3	0.12	1.01	0.30	0.89	Cr	54	3405	126	3672
Fe_2O_3	6.22	5.85	1.69	12.27	Cu	65	33	39	10
FeO	2.24	4.15	0.69	2.83	Ga	1	0	1	0
MnO	0.02	0.08	0.08	0.15	Nb	4	4	4	2
MgO	0.07	0.96	0.15	0.47	Ni	36	1243	0	1361
CaO	0.04	0.12	0.06	0.14	Pb	0	0	5	0
Na_2O	0.44	0.84	0.13	0.57	Rb	3	2	1	2
K_2O	0.00	0.00	0.14	0.03	Sn	16	5	5	1
P_2O_5	0.02	0.00	0.15	0.03	Sr	5	0	0	3
H_2O^+	1.12	0.87	0.29	0.41	V	101	50	254	60
H_2O^-	0.22	0.33	0.02	0.36	Y	1	13	10	18
CO_2	0.10	0.09	0.07	0.15	Zn	84	79	9	60
SO_3		0.50		0.01	Zr	36	33	1	9
$Fe^{3+}/(Fe^{2+}+Fe^{3+})$	0.74	0.59	0.65	0.81					
Total	98.28	99.04	98.03	100.38					

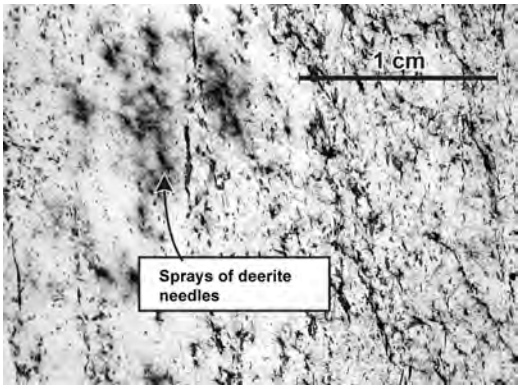

FIG. 2. Deerite-bearing sample M562 (plane-polarized light). Unoriented needles of deerite and riebeckite are found throughout the rock, but are concentrated in sprays and clusters accentuated by quartz-rich coronas poor in Fe-rich minerals. These clusters overprint an older schistose fabric characterized by platelets of Fe oxide and oriented idioblasts of zoned sodic amphibole. In the photomicrograph shown, the amphiboles are oriented predominantly with *c* perpendicular to the plane of the section.

quartz-rich, massive, macroscopically almost featureless rock in which penetrative shearing has almost destroyed the original compositional layering. Thin trails of mafic minerals festoon shear planes separating wide quartz-rich microlithons. An older generation of coarse, aligned blue amphibole exhibits very complex zoning. As in M562 and G2074, this rock also contains a younger generation of minute, unoriented bluish and brownish crystallites. Analysis was not possible. Relics of garnet are observed. Sample G2079 exhibits a particularly prominent segregation into quartz-rich and dark, spinel-rich layers. These dark layers also contain abundant amphibole, aegirine, garnet and Cr-rich spinel. In comparison to the previous samples, this rock is relatively rich in macroscopically conspicuous white K-mica oriented in the plane of the foliation.

After the discovery of deerite at Buenos Aires, 13 samples of metachert from the historical Loma de los Guapos eclogite locality (Somin and Millán, 1981; Hatten *et al*., 1988) in the western Trinidad dome were also examined. The quartz matrix of these rocks also encloses blue amphibole needles, but these metacherts are poorer in Fe and Fe oxide minerals are subordinate. Almost all samples contain garnet. In contrast to the metaquartzites of Buenos Aires,

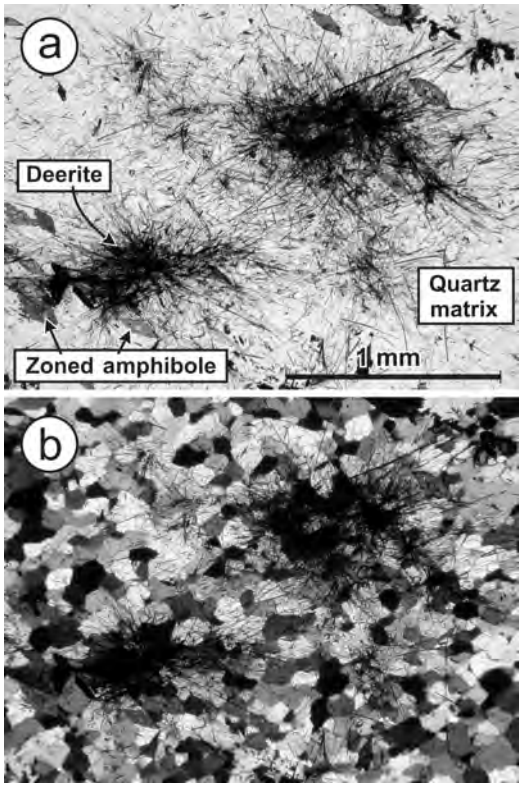

FIG. 3. Sprays and bundles of deerite and associated riebeckite in sample M562 (*a*: plane polarized light; *b*: crossed polarizers). Note the characteristic polygonal fabric ('foam structure') of the quartz matrix indicating stress-free annealing.

these rocks commonly contain graphite and rutile. None were found to contain deerite, so that this suite of samples was not investigated further.

Bulk-rock chemical composition

Bulk-rock chemical composition was obtained by X-ray fluorescence with a Philips PW 1400 spectrometer. Uncertainties are estimated to be ±1% for major and ±10% for minor elements of importance. FeO was determined potentiometrically (Ungethüm, 1965), and Fe_2O_3 by difference. H_2O and CO_2 were analysed coulometrically (Johannes and Schreyer, 1981).

The bulk composition of all metaquartzites is clearly dominated by SiO_2 and Fe_2O_3 + FeO (Table 2). Together, these oxides already sum to between 94 and 97 wt.% of the total content of the rock. The state of oxidation is high, with

$Fe^{3+}/(Fe^{2+}+Fe^{3+})$ varying between 0.59 and 0.81. The MnO content is consistently low. The most Fe-rich sample G2079, with an Fe_2O_3 content of 12.27 wt.%, is also the one containing the Fe^{3+}-rich pyroxene aegirine. High Cr contents in G2074 and G2079 correlate with the appearance of a Cr-rich spinel.

Mineral compositions

Representative analyses of minerals are summarized in Tables 3 and 4. Microprobe analyses were obtained with a Cameca SX 50 at 15 kV acceleration voltage and 10 nA beam current, 20 s counting time (10 s on background), aided by beam scans at 15 kV and 40 nA. Data correction followed the PAP procedure (Pouchou and Pichoir, 1984). Element mapping was carried out using a CAMECA Camebax. The standards employed were natural pyrope for Si, Al, Mg; natural spessartine for Mn; natural jadeite for Na; natural rutile for Ti; synthetic andradite for Fe, Ca; synthetic potassium silicate and barium silicate glass for K and Ba, respectively; synthetic oxides of Cr, Ni, Cu and Zn for the respective elements.

Deerite

Considerable substitution on the divalent and trivalent Fe sites in the end-member deerite formula $Fe^{2+}_{12}Fe^{3+}_{6}Si_{12}O_{40}(OH)_5$ is possible (see summary by Deer *et al*., 1997), whereby the most extensive possibility is that of Mn^{2+} for Fe^{2+}. Although Langer *et al*. (1977) synthesized a solid-solution series from the above end-member to a composition with 20% Al for Fe^{3+}, such high Al contents are generally found in nature only in combination with Ti (e.g. Vernié *et al*., 1986). Up to 10% of Fe^{2+} can be replaced by Mg (Vernié *et al*., 1986). The present data (Table 3) are shown in Fig. 4 in the representation introduced by Vernié *et al*. (1986). All analyses indicate >95% end-member compositions, and the deerites of

TABLE 3. Representative deerite analyses from samples M562 and G2074*.

Sample	M562	M562	G2074	G2074
Analysis no.	10566/6	10566/14	11069/22	11069/23
SiO_2	33.08	32.77	33.33	32.79
TiO_2	0.14	0.14	0.24	0.19
Al_2O_3	0.12	0.15	0.53	0.35
Fe_2O_3	22.14	22.41	21.49	22.89
Cr_2O_3	0.06	0.00	0.51	0.51
FeO	38.79	38.53	37.23	36.59
MnO	0.37	0.30	0.95	0.89
MgO	0.10	0.07	0.92	0.91
CaO	0.03	0.02	0.04	0.05
Na_2O	0.06	0.06	0.04	0.04
K_2O	0.02	0.01	0.00	0.01
Sum	94.89	94.46	95.28	95.21
Si	11.944	11.896	11.884	11.736
Ti	0.038	0.037	0.064	0.051
Al	0.049	0.064	0.223	0.148
Fe^{3+}	6.016	6.121	5.766	6.165
Cr	0.016	0.000	0.144	0.144
Fe^{2+}	11.712	11.698	11.101	10.952
Mn	0.113	0.091	0.287	0.270
Mg	0.053	0.035	0.489	0.486
Ca	0.011	0.008	0.015	0.019
Na	0.039	0.044	0.028	0.028
K	0.007	0.006	0.000	0.002

* Number of ions on the basis of 45 oxygens; Fe^{2+}/Fe^{3+} obtained by normalizing sum of cations to 30.000.

TABLE 4*a*. Representative electron microprobe analyses of spinel, garnet, phengite and chlorite*.

Sample	G2074-Spinel			G2077-Garnet			G2077-Phengite		G2074-Chlorite	
Analysis no.	1060815a/1	1060815a/2	1060815a/4		11089/83	11089/90		11088/12		11475/24
Comment	core	rim no. 1	rim no. 2		core	rim				
SiO_2	0.05	0.06	0.14	SiO_2	37.02	37.00	SiO_2	48.06	SiO_2	25.47
TiO_2	0.01	0.04	0.01	TiO_2	0.00	0.00	TiO_2	0.02	TiO_2	0.00
Al_2O_3	25.96	1.62	0.03	Al_2O_3	19.79	20.86	Al_2O_3	23.41	Al_2O_3	17.14
Cr_2O_3	35.82	33.74	0.80	Cr_2O_3	0.02	0.08	Cr_2O_3	0.02	Cr_2O_3	0.90
Fe_2O_3	2.45	32.36	68.77	Fe_2O_3	1.77	0.40	MgO	1.99	MgO	10.80
MgO	0.30	0.06	0.03	MgO	0.28	0.79	FeO	9.74	FeO	31.02
FeO	32.42	29.32	30.91	FeO	11.07	21.68	MnO	0.08	MnO	0.49
MnO	0.30	1.46	0.03	MnO	22.78	12.74	CaO	0.00	NiO	1.74
ZnO	3.35	0.65	0.00	CaO	7.44	6.66	BaO	0.28	CaO	0.10
CaO	0.04	0.00	0.01	Sum	100.17	100.21	Na_2O	0.12	Na_2O	0.07
Sum	100.70	99.31	100.73				K_2O	10.43	K_2O	0.05
							Sum	94.15	Sum	87.78
Mg	0.015	0.001	0.002	Si	3.000	2.986				
Fe^{2+}	0.892	0.937	0.986	Al	1.891	1.985	Si	3.397	Si	5.643
Mn	0.008	0.043	0.001	Ti	0.000	0.000	^{IV}Al	0.603	^{IV}Al	2.357
Zn	0.081	0.015	0.000	Cr	0.001	0.005	Sum	4.000	Sum	8.000
Ca	0.001	0.000	0.000	Fe^{3+}	0.108	0.024				
Ti	0.000	0.001	0.000	Sum	2.000	2.013	^{VI}Al	1.347	Al^{VI}	2.119
Si	0.002	0.002	0.005				Ti	0.001	Ti	0.000
Sum	0.999	0.999	0.994	Mg	0.033	0.095	Cr	0.001	Cr	0.158
				Fe^{2+}	0.750	1.464	Mg	0.210	Mg	3.567
Al	1.007	0.090	0.001	Mn	1.564	0.871	Fe^{2+}	0.576	Fe^{2+}	5.748
Cr	0.932	0.976	0.024	Ca	0.646	0.576	Mn	0.005	Mn	0.092
Fe^{3+}	0.061	0.933	1.974	Sum	2.993	3.006	Sum	2.140	Ni	0.310
Sum	2.000	1.999	1.999						Ca	0.024
							Ca	0.000	Na	0.030
							Ba	0.007	K	0.014
							Na	0.016	Sum	12.062
							K	0.941		
							Sum	0.964		

* Spinel: number of ions on the basis of 4 oxygens, Fe^{2+}/Fe^{3+} obtained by iterative optimization of stoichiometry; garnet: number of ions on the basis of 12 oxygens, Fe^{2+}/Fe^{3+} obtained by normalizing total cations less divalent cations to 5.000; phengite: number of ions on the basis of 11 oxygens, all Fe assumed to be divalent; chlorite: number of ions on the basis of 28 oxygens, all Fe assumed to be divalent.

TABLE 4*b*. Representative electron microprobe analyses of amphibole*.

Sample	M562	M562	M562	G2074	G2074
Analysis	10614/9	10614/3	10615/42	11477/1	11477/3
Comment	inner core	outer core	rim	core	rim
SiO_2	56.11	54.78	51.33	54.05	53.64
TiO_2	0.0	0.0	0.0	0.06	0.01
Al_2O_3	7.08	6.23	2.5	4.76	4.65
Cr_2O_3	0.0	0.08	0.04	0.62	0.08
Fe_2O_3	9.11	9.00	15.54	9.93	10.25
FeO	6.63	12.32	20.30	15.41	14.99
MnO	0.13	0.25	0.41	0.03	0.06
MgO	9.24	5.94	0.45	4.35	5.08
NiO	0.92	0.77	0.0	0.94	0.41
ZnO	0.93	0.68	0.09	0.0	0.03
CaO	0.31	0.3	0.2	0.22	0.74
Na_2O	7.2	7.04	6.66	6.94	6.67
K_2O	0.01	0.01	0.01	0.01	0.02
Sum	97.67	97.40	97.53	97.32	96.63
Si	7.891	7.929	7.826	7.955	7.929
^{IV}Al	0.109	0.071	0.174	0.045	0.071
Sum	8.000	8.000	8.000	8.000	8.000
^{VI}Al	1.065	0.991	0.275	0.781	0.740
Fe^{3+}	0.986	1.000	1.858	1.127	1.169
Cr	0.000	0.009	0.005	0.072	0.009
Mg	1.937	1.282	0.102	0.954	1.120
Fe^{2+}	0.796	1.524	2.697	1.944	1.901
Mn	0.015	0.031	0.053	0.004	0.008
Ni	0.104	0.090	0.000	0.111	0.049
Zn	0.097	0.073	0.010	0.000	0.003
Sum	5.000	5.000	5.000	5.000	5.000
Ca	0.047	0.047	0.033	0.035	0.117
Na *M*4	1.953	1.953	1.967	1.965	1.883
Sum	2.000	2.000	2.000	2.000	2.000
Na *A*	0.010	0.022	0.001	0.015	0.029
K	0.002	0.002	0.002	0.002	0.004
Sum	15.012	15.024	15.003	15.017	15.033

* Number of ions on the basis of 23 oxygens; Fe^{2+}/Fe^{3+} obtained by normalizing sum of cations less Ca, Na, K to 13.000.

sample M562 are among the closest to end-member composition reported so far. Muir Wood (1979) reported deerite from the Franciscan with lower Al contents, but these analyses also show considerably higher Mn^{2+}. Some Alpine deerites have comparably low Mn^{2+} and Mg, but these contain considerably more Al (Deer *et al*., 1997). In keeping with the relatively high bulk Cr content in G2074 (Table 2), the deerite from this sample contains 0.51 Cr_2O_3.

Hematite and minerals of the spinel group

Considerable discussion has accompanied the question of deerite stability with respect to f_{O_2} and the Fe oxide minerals that can coexist with

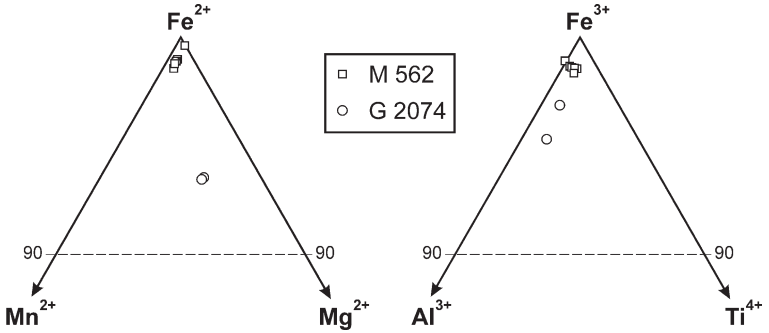

FIG. 4. Major substitutional deviations from end-member ferrous-ferric deerite, plotted as suggested by Vernié *et al.* (1986).

this mineral. Although Vernié *et al*. (1986) claimed to have found deerite coexisting with hematite in highly oxidized metasediments, experimental investigations on deerite (Langer *et al*., 1977; Lattard and Le Breton, 1994) suggest that deerite can be stable together with hematite only at very low temperatures of metamorphism. Similarly, the work of Okay (1980, 1987), Owen (1988) and Evans and Owen (2002) suggests that at the given temperatures of metamorphism in the Escambray Massif (Grevel, 2000), the Mg-Al-poor riebeckite coexisting with the deerite should not be stable in the presence of hematite. It is therefore of considerable importance to document and evaluate the fact that in the present study there is clear evidence for the presence of hematite in the early metamorphic history of the deerite-bearing metacherts.

Table 1 indicates that, in keeping with the Fe-rich bulk compositions (Table 2), Fe oxides are an important part of the basic mineral assemblages observed. For the samples studied in detail (Table 1), reflected light microscopy indicates that secondary martitization is ubiquitous ('late hematite' in Table 1). However, in the deerite-containing sample M562, and also in sample G2077 in which deerite is almost certainly present, there is definite evidence of early hematite growth in the history of the rock. The aspect of the opaque Fe oxide mineral in M562 is that of platelets of hematite, reaching 500 μm in diameter. There are no unequivocal sections of opaque minerals suggesting primary cubic crystals of a spinel-like phase. These opaque platelets are rigorously oriented in the plane of the dominant foliation of the rock, as are the sodic amphiboles (Fig. 2). Some platelets are bent. They also occur as inclusions in the cores of these idioblasts of sodic amphibole. Reflected light microscopy indicates that the large platelets exceeding 100−150 μm are almost all essentially hematite, with occasional rare patches of magnetite. In contrast, many of the smaller platelets, <100 μm, consist partially to totally of magnetite, and appear to represent pseudomorphs after hematite, although these again show varying degrees of subsequent martitization (Fig. 5). In quartz-rich sample G2077 the total amount of opaques is much smaller. Almost all grains of Fe oxide are magnetite with typical spinel cube-octahedron habitus, but some very small platelets of hematite can be found. In both M562 and G2077 the magnetite and hematite are, within the detection limits of the electron microprobe, pure Fe oxides.

In deerite-bearing sample G2074, and also in G2079 without deerite, the platelets are comple-

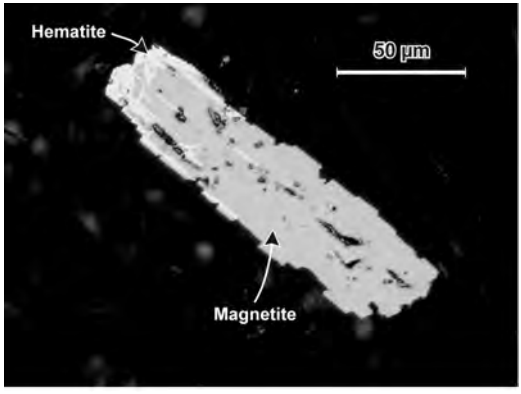

FIG. 5. Magnetite pseudomorph of primary hematite platelet in sample M562 (reflected light, oil immersion). Note martitization beginning in upper left termination of the crystal.

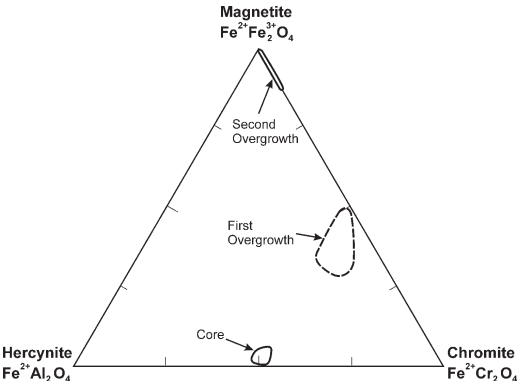

FIG. 6. Composition of zoned spinel-group minerals in samples G2074 and G2079 projected onto the plane magnetite-chromite-hercynite. See Fig. 7.

tely absent. Crystals of opaques show the typical cross-section of cubic spinel. These rocks contain ~3500 ppm Cr (Table 2), and discontinuous compositional zoning of the spinel crystals is characteristic (Fig. 6), with similar trends in both rocks. Compositions can be expressed to more than 90–95% in terms of the end-members hercynite, chromite and magnetite, and have been projected into this solid-solution plane in Fig. 6. The cores of the spinel grains are ~50/50 solid solutions of hercynite-chromite. These cores are overgrown by 50/50 chromite-magnetite and then by chromiferous magnetite in the rims. Between 1 and 10% of Fe^{2+} may be substituted by Mn^{2+} and Mg. No systematic trends were observed in the extent of this substitution.

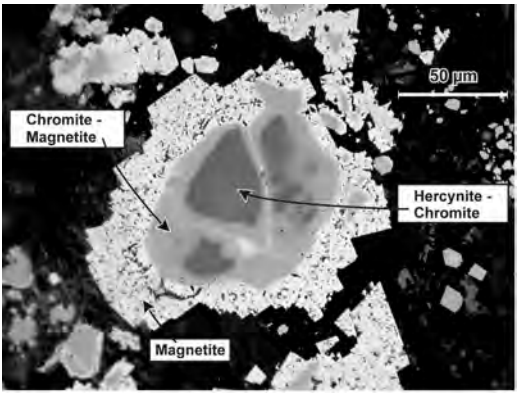

FIG. 7. Zoned spinel crystal from sample G2074 (reflected light, oil immersion). For compositions see Fig. 6.

Amphibole

All analysed amphiboles belong to the sodic amphibole group (Leake *et al*., 1997, 2004). The sum of all calcic end-members is generally <<10%. The same is true for the *A*-site content, so that the analyses are well represented in the classical glaucophane-ferroglaucophane-riebeckite-magnesioriebeckite compositional plane (Fig. 8). In some cases Ni, Cr and Zn are above the detection limit, especially in M562 and G2074, but total contents never exceed 0.05 to 0.10 a.p.f.u.. Accurate determinations of the compositions of the younger, unoriented needles of the recrystallized matrix are difficult. However, qualitative analyses indicate that these amphiboles are very Mg- and Al-poor and correspond closely to end-member riebeckite. Such compositions are analogous to the thin outer rims of the older generation amphiboles in M562 and G2077 and may be coeval with these rims.

Unzoned sodic amphibole is found only in deerite metachert G2074 (Fig. 8), where the composition is Al-rich riebeckite (or 'crossite' in the classical terminology of Miyashiro, 1957), but G2079 is also only slightly zoned (Fig. 9). In contrast, the large, older-generation amphiboles in M562 and G2077 exhibit strong and discontinuous zoning (Figs 10, 11), ranging from Al-poor glaucophane in the core to riebeckite end-member composition at the rim. The overall zoning trend in M562, G2077 and G2079 is from glaucophane towards end-member riebeckite, but it is noteworthy that the zoning in G2077 is in part reverse. Overgrowths are sharply defined and in part obviously followed periods of resorption.

Because ambient oxygen fugacity plays an important role in defining the stability of deerite, independent information on f_{O_2} from sodic amphibole composition is important. The information provided by Okay (1980, 1987), Owen (1988) and Evans and Owen (2002), both in terms of empirical analysis of natural occurrences as well as experimental work on near-end-member riebeckite, suggests that the unoriented Mg-Al-poor riebeckite needles coexisting with deerite and the riebeckite-rich rims of the large idioblastic amphibole crystals should not be stable together with hematite. These compositions are compatible only with magnetite.

Garnet

Garnet in the metacherts is strongly zoned (Fig. 12). Cores containing up to 70 mol.%

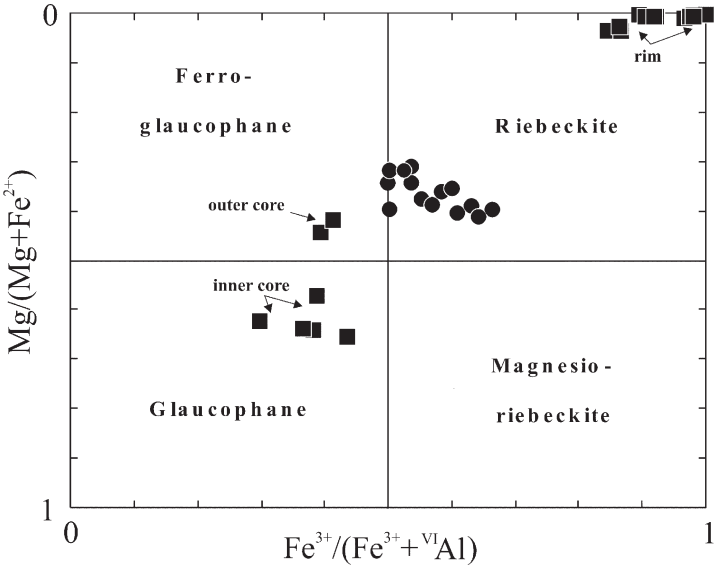

FIG. 8. Composition of sodic amphiboles in deerite-bearing metacherts M562 (filled squares) and G2074 (filled circles). Nomenclature according to Leake *et al.* (1997).

spessartine grade to rims with 60–70 mol.% almandine. Pyrope and grossular contents remain relatively constant at ~5 mol.% and 10–20 mol.%, respectively. Small remnants of garnet in chlorite pesudomorphs in sample G2074 allow only spot analyses.

Additional minerals

Phengite is present in samples G2077 and G2079. In keeping with the high-pressure character of these rocks, the Si contents depart significantly from 3.0 in the ideal muscovite formula $KAl_2[Si_3AlO_{10}](OH)_2$ (Massonne and Schreyer,

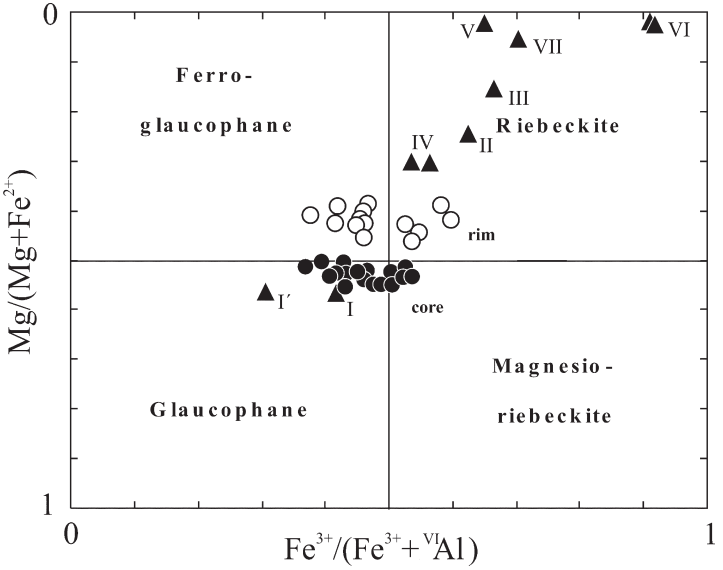

FIG. 9. Composition of sodic amphiboles in metacherts G2077 (filled triangles) and G2079 (circles). The Roman numerals are keyed to the growth zones in Fig. 11. Nomenclature according to Leake *et al.* (1997).

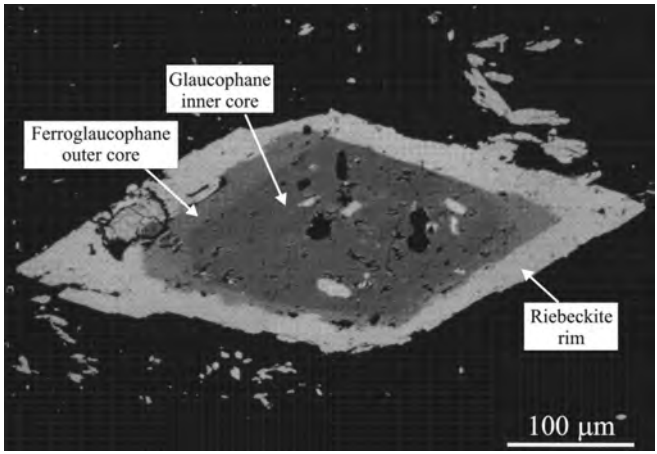

FIG. 10. Back-scattered electron (BSE) image of zoned amphibole in deerite metaquartzite M562. For compositions see Fig. 8.

1987). Phengite in G2077 averages 3.4 Si p.f.u., and 3.3 p.f.u in G2079. A number of analyses in G2079 show deviations from the ideal Tschermaks substitution, indicating replacement of octahedral Al by Fe^{3+}.

In the metaquartzite samples studied here, chlorite is found only in G2074, where it has replaced garnet and amphibole. According to AIPEA recommendations (Bailey, 1980), this is an Fe^{2+}-dominant trioctahedral chlorite consisting of 63% chamosite (Fe^{2+}-end-member), 33% clinochlore (Mg-end-member), 3% nimite (Ni-end-member) and 1% pennantite (Mn-end-member). Cr replaces up to 6% of the octahedral Al. The Ni and Cr contents are notable and presumably responsible for the conspicuous pleochroism observed in thin-section.

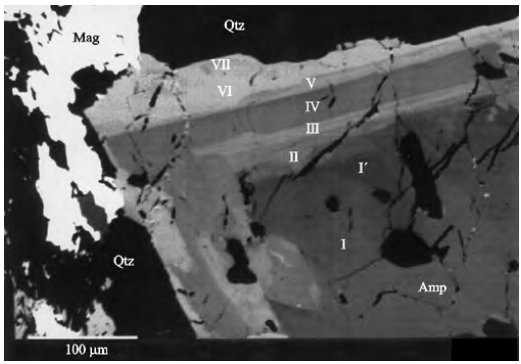

FIG. 11. BSE image of zoned amphibole in metaquartzite G2077. For compositions see Fig. 9.

Clinopyroxene in sample G2079 is aegirine, with 25% to 35% jadeite component. The high aegirine component reflects the very high Fe_2O_3 content of 12.27 wt.% in this rock (Table 2) .

P-T-f_{O_2} conditions

Oxidation state

Although hematite is now present in the deerite-bearing rocks, petrographic interpretation indicates that deerite did not coexist stably with this mineral, as suggested by Vernié *et al*. (1986) for a deerite occurrence in the schistes lustrées of Corsica. Martitization ('late hematite' in Table 1; see Figs 5, 7) is a common late-stage feature of many magnetite-bearing rocks (e.g. Ramdohr, 1980), and appears to have little to do with deerite stability in the present case. On the other hand, the platelets of Fe oxide found in M562 and to a lesser extent in G2077 clearly exhibit the morphology to be expected of primary hematite growth. The growth of these hematite platelets is associated with the growth of glaucophane, and the platelets form common inclusions in these amphiboles. As pointed out by Okay (1987) and Owen (1988), the core compositions of glaucophane, ferroglaucophane and Mg-Al-rich riebeckite ('crossite') in M562 and G2077 are compatible with hematite stability. This is also true of the amphibole cores in the samples studied by Vernié *et al*. (1986). However, as pointed by Okay (1987), the compositional zoning trend in the Corsican samples is towards riebeckite, pointing to more reducing conditions

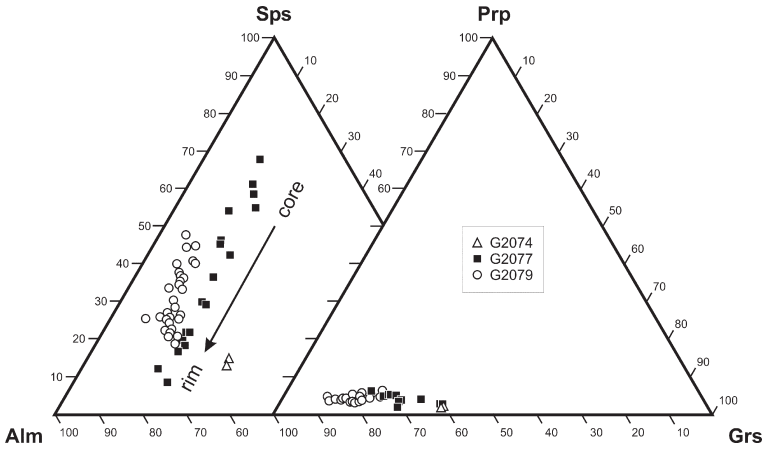

FIG. 12. Compositional variation in garnet (molecular proportions). Sps: spessartine; Alm: almandine; Prp: pyrope; Grs: grossular.

during the course of progressive metamorphism. The same is true in M562 and G2077, where the increasingly more riebeckitic compositions (Figs 8, 9) are stable only at oxidization states compatible with magnetite (Okay, 1980, 1987; Owen, 1988; Evans and Owen, 2002). As already described above, deerite growth is contemporaneous with needles of sodic amphibole of almost end-member riebeckite composition. Both the riebeckite and deerite needles form unoriented sprays in a recrystallized quartz matrix with equilibrium 'foam' fabric (Fig. 3). By contrast, the large glaucophane idioblasts and hematite platelets are older than the deformation that led to the dominant foliation (Fig. 2). We therefore suggest that the magnetite now found in M562 and G2077 formed by recrystallization of primary hematite, and also represents the stable Fe oxide that coexisted with deerite. We can offer no explanation for the fact that the large platelets generally consist primarily of hematite whereas the small platelets are essentially magnetite. It is possible that the larger platelets did not react completely with magnetite, or that the smaller platelets were less prone to secondary martitization. Unfortunately there is no way of distinguishing primary 'early hematite' from 'late hematite' formed by martitization in the large platelets.

Oxygen isotope thermometry

From the foregoing, there seems little doubt that the experimental results and the stability analysis of Lattard and Le Breton (1994) for end-member deerite are valid, and that deerite coexisted with magnetite. Thus the oxygen isotope fractionation between quartz and magnetite should be the method of choice for determining the metamorphic temperatures at which deerite grew.

Theoretically, quartz and magnetite represent the ideal mineral pair for deriving equilibration temperatures from oxygen isotope fractionation. Of all known minerals, quartz is the phase which concentrates ^{18}O the most, and magnetite is the phase with the lowest ^{18}O content in any known assemblage with the exception of perovskite (see Chacko *et al*., 2001, for example). Thus, the quartz-magnetite fractionation is the largest of any silicate-silicate/oxide combination.

Two fractions of both quartz and magnetite from the deerite-bearing metaquartzite sample S149 (see Table 1), were used for oxygen isotope analysis, i.e. a coarse 40–60 μm and a fine <40 μm fraction for magnetite and a coarse 80–350 μm and a fine <80 μm fraction for quartz. These were collected by hand-picking from grain fractions <80–350 μm for quartz and <40–100 μm for magnetite obtained by standard methods for quartz separation. Magnetite was further purified from intergrown silicate impurities by repeated grinding in an agate mortar under alcohol and removing the magnetite with a hand magnet.

8–10 mg aliquots of the separates were reacted with purified F_2 gas (Asprey, 1976) in Ni-bombs at an F_2 pressure of 2 bar and temperatures of 550–600ºC for quartz and 600–650ºC for

magnetite, at reaction times of 12 to 15 h. The liberated oxygen was converted to CO_2 following the technique of Clayton and Mayeda (1963); reaction yields were controlled volumetrically and are typically 95–100% for quartz and 90–100% for magnetite. The CO_2 was analysed using a Sira-9 triple collector mass spectrometer by VG-isogas.

The results of oxygen isotope analysis are presented in Table 5. There is a pronounced difference between the two magnetite fractions and a corresponding, albeit smaller difference in the quartz fractions, indicating that complete separation of oxide and silicate was not yet achieved at the scale of the coarser fractions. The coarser magnetite fraction is obviously still markedly contaminated by heavier $\delta^{18}O$ from the silicate, and the coarser quartz fraction also shows some influence from lighter magnetite. From the foregoing it is also clear that the most efficient separation of magnetite from intergrown hematite will be achieved with the finer grain-size fraction. Although there is no oxygen isotopic fractionation between magnetite and hematite, any 'early' hematite still present in the larger platelets will not have equilibrated with the younger quartz fraction measured and should be avoided. We assume that the martitization of the smaller platelets (e.g. Fig. 4) will be a predominantly solid-state reaction, and the additional oxygen necessary is ~10% of the oxygen already present. This effect should be minor.

The data in Table 5 can be used to estimate temperatures of equilibration via the fractionation equation

$$1000\ \ln\alpha = A10^6/T^2\ (K)$$

where A is the fractionation coefficient of 6.29 for quartz-magnetite (Chacko *et al*, 2001). The fractionation 1000 $\ln\alpha_{(qtz\text{-}mag)}$, usually only estimated from the difference of the δ values, can be precisely calculated according to

$$a_{A\text{-}B} = \frac{1000+\partial_A}{1000+\partial_B}$$

and yields values for 1000 $\ln\alpha_{(qtz\text{-}mag)}$ of 10.00 and 11.49 for the coarse and fine fractions, respectively. The corresponding temperatures of equilibration are 520 (coarse fraction) and 467ºC (fine fraction). We conclude that a temperature of ~470ºC is the best value for isotopic equilibration between magnetite and quartz crystallizing together with deerite in sample M562/S149.

An analytical uncertainty of ±0.2‰ results in a temperature ambiguity of only ±6ºC in the temperature range of interest. A more pronounced uncertainty arises from differences due to contrasting experimental calibrations. However, there appears to be a consensus in the stable isotope community to accept the results of the mineral-calcite exchange experiments introduced by the Clayton group (Chicago) as preferable to those of older mineral-water exchange experiments. The fractionation coefficient for quartz-magnetite of 6.29 used in this paper is based on the experiments of Clayton *et al*. (1989) and Chiba *et al.* (1989), compiled recently by Chacko *et al.* (2001). Another factor leading to problems in the interpretation of oxygen isotope temperatures can result from diffusional exchange after the crystallization of a mineral phase. However, this factor can be ignored at greenschist-facies temperatures, as shown by Valley (2001), who recently provided a comprehensive discussion of oxygen isotope thermometry.

TABLE 5. Results of oxygen isotope analysis.

Mineral	Grain size (μm)	$\delta^{18}O$	2σ
Magnetite	40–60	4.9	0.01
Magnetite	<40	3.7	0.2
Quartz	80–350	15.0	0.03
Quartz	<80	15.3	0.02

Pressure estimates from the stability field of end-member deerite

Because the deerite observed in sample M562 corresponds very closely to the ferrous-ferric end-member (Table 3), the comprehensive study of Lattard and Le Breton (1994) on the *P-T-*f_{O_2} stability of this composition represents an invaluable aid in estimating the metamorphic crystallization conditions of the deerite-bearing metacherts. Lattard and Le Breton (1994) summarized and augmented available experimental data and information from natural occurrences. Their *P-T* phase-boundary is given in Fig. 13. At a temperature of 470ºC, minimum pressures of ~15 kbar are required to stabilize end-member deerite. The critical constraint to be derived is the fact that, independent of absolute pressure, the formation of deerite in the metacherts of the Escambray Massif requires

geothermal gradients of <10°/km, i.e. active subduction.

f_{O_2} conditions

Lattard and Le Breton (1994) show that deerite stability is critically dependent on a very specific, restricted range of oxygen fugacities close to the quartz-fayalite-magnetite buffer. On the basis of a temperature of 470ºC and pressures of 15−16 kbar (Fig. 13), this translates to an f_{O_2} of ~−23 bar (Lattard and Le Breton, 1994, their Fig. 8)

Discussion

Crystal chemistry

Although Muir Wood (1979) suggested, on the basis of the deerite analyses available to him at the time, that there might be regional compositional differences allowing 'Franciscan' and 'Alpine' types of deerite to be distinguished, such categories have become blurred as more and more analyses have become available (see summary by Deer *et al*., 1997; see also Schliestedt, 1980; Worthing, 1987; Dudek and Kienast, 1987; Kienast, 1983; Klein-Helmkamp, 1996; for further analyses). Muir

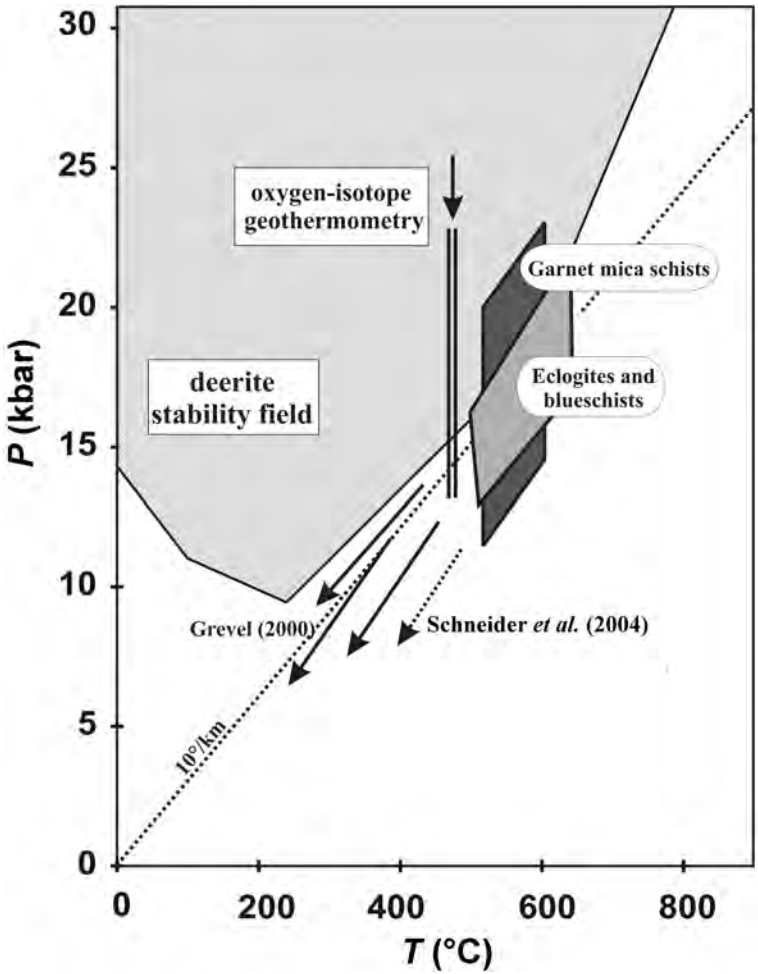

FIG. 13. Deerite stability field after Lattard and Le Breton (1994) and oxygen isotope geothermometry of this study constrain *P-T* conditions of stress-free annealing of metacherts of the Gavilanes unit to ~470ºC and >15 kbar. Also shown are *P-T* determinations of garnet mica schists and metabasites of the Gavilanes nappe after Grevel (2000). Arrows indicate exemplary exhumation trajectories for several samples of the metachert unit from Grevel (2000) and Schneider *et al*. (2004).

Wood (1979) suggested that 'Franciscan' deerites are particularly Mn^{2+}-rich, but the most manganoan deerites now known are from the Aegean (Reinecke, 1987).

As Muir Wood (1979) noted, local metamorphic conditions such as pressure, temperature, oxygen fugacity, etc. will play a key role in defining the composition of deerite; nevertheless, the near-end-member chemistry of the deerites from the Escambray appear to be primarily dictated by the bulk-rock compositions (Table 2), which are extremely poor in Al_2O_3, MgO, MnO and TiO_2. Indeed, the deerite from M562, which is the closest to the ferrous-ferric end-member, also correlates with contents of only 0.12 wt.% Al_2O_3, 0.07 wt.% MgO, 0.02 wt.% MnO and 0.01 wt.% TiO_2 in the rock. In addition, the overgrown glaucophane cores of the first-generation oriented sodic amphibole will have sequestered much of the originally available Al_2O_3 and MgO, so that the effective bulk composition of the rock during later deerite growth will have been even lower in these components.

The zoned garnet and spinel crystals suggest Rayleigh-type growth fractionation of Mn and Cr (e.g. Hollister, 1966) and early closed-system conditions. As noted above, the large oriented sodic amphiboles also effectively isolate Mg and Al in their cores, indicating as well that these amphiboles started growth already well within blueschist facies *P-T* conditions. However, the complex and in part oscillatory zoning in the outer regions of these amphibole crystals, as well as the evidence for intermittent resorption (e.g. Figs 9–11), are more in accord with open-system conditions during subsequent stages along the *P-T* path (e.g. Yardley *et al*., 1991). As Lattard and Le Breton (1994) demonstrated, deerite stability is very restricted with respect to f_{O_2} conditions. Either there was a return to closed-system conditions, with internal buffering by the deerite-bearing assemblage itself, or the infiltrating fluid must have precisely imposed the necessary f_{O_2} conditions. This necessity, in conjunction with the severe requirements stipulated for the bulk rock composition, are probably the primary reason for deerite scarcity even within fairly similar metacherts with analogous *P-T* histories in the Escambray Massif.

P-T-f_{O_2} conditions

Available thermobarometric estimates for rocks of the Gavilanes unit are summarized in Fig. 13. The data of Grevel (2000) are grouped for eclogites and blueschists (14 samples) and garnet mica schists (seven samples). Broadly speaking, exchange thermometers such as the Fe-Mg distribution between omphacite and garnet yield temperatures between 500 and almost 700ºC, in general reflecting various stages of re-equilibration along a dynamic exhumation *P-T*-path. Where multi-equilibrium calculations with critical phase assemblages are possible, garnet mica schists yield 16–23 kbar and 530–610ºC (Grevel, 2000). Results for eclogites group at similar pressures of 16–20 kbar but slightly higher temperatures of 580–630ºC. These conditions are the best available estimates of peak metamorphic conditions, but may not necessarily reflect maximum subduction depths. Schneider *et al*. (2004) investigated three eclogites from outcrops of the Gavilanes nappe (using our nomenclature). Their estimates of 600–650ºC and minimum pressures of 15–16 kbar (Schneider *et al*., 2004, p. 239) are in accord with the results of Grevel (2000), but lie at the lower end of Grevel's estimated pressure range.

The combination of the deerite stability field and the results of oxygen isotope geothermometry (Fig. 13) lead to estimated *P-T* conditions for deerite growth of ~470ºC and a minimum of ~15 kbar. These temperatures are distinctly lower than those derived by mineral thermobarometry for the garnet mica schists and metabasites (Grevel, 2000; Schneider *et al*., 2004). However, temperatures of ~470ºC from quartz-magnetite oxygen isotope fractionation are also supported by the results of carbon isotope fractionation in the graphitic metacarbonates representing the matrix and volumetric bulk of the Gavilanes unit (Maresch, Hoernes *et al*., in prep.). The minimum pressures obtained from the deerite stability field are also somewhat higher than those suggested for the retrograde exhumation paths of the garnet mica schists and basic rocks (Fig. 13). Nevertheless, we suggest that all these results can be interpreted in terms of a common geodynamic scenario. On the one hand, the exhumation paths in Fig. 13, even if the uncertainties in thermobarometry are acknowledged, provide testimony to considerable heterogeneity in the exhumation histories of rocks in the Gavilanes nappe, in keeping with their structural interpretation as a 'mega-mélange'. The Gavilanes nappe must therefore have been assembled during exhumation. On the other hand, all exhumation paths in Fig. 13 show steep, 'cold' *P-T* gradients.

Subduction must still have been active during exhumation. It is, moreover, logical to assume that quartz- and carbonate-rich lithologies will remain ductile, deformable and susceptible to re-equilibration to much lower temperatures than other lithologies. Deerite is a late product during stress-free annealing in the metacherts and presumably represents a stage in the exhumation process when penetrative deformation becomes heterogeneous and is restricted to specific shear zones. As noted by Fiorentini *et al*. (1990), the stress-induced recrystallization of the quartz matrix coexisting with magnetite and deerite should be a prime driver of isotopic equilibration. Thus the lower temperatures in the deerite assemblage appear logical. The greater pressures indicated by the deerite stability field for the retrograde path of the metacherts appear to be robust and convincing constraints. The critical terminal reaction between 250 and 600ºC (Lattard and Le Breton, 1994) is deerite = grunerite + magnetite + quartz + H_2O. Lowered water activity will drive the reaction to even higher pressures. Because sodic amphibole and magnetite coexist with deerite, we have also attempted to calculate the above reaction in terms of a sliding equilibrium. However, the grunerite component in the riebeckites is too small and swamped by uncertainties in Fe^{2+}/Fe^{3+} estimation in the amphibole. In any case, lowering the activity of grunerite by solid solution will again drive the equilibrium to the high-pressure side. We therefore conclude that the deerite-bearing metacherts provide particularly clear-cut constraints for active subduction during exhumation. As stated by Lattard and Le Breton (1994) and indicated in Fig. 13, deerite stability requires a thermal gradient of <10ºC/km, indicative of a 'cold', mature subduction zone.

Acknowledgements

We are indebted to Guillermo Millàn, Havana, who introduced us to the Escambray Massif and gave us valuable assistance in the early stages of this project. Heinz-Jürgen Bernhardt and Olaf Medenbach provided critical and indispensable help in our attempts to unravel the crystallization histories of the Fe oxides in our deerite-bearing rocks. We thank Dominique Lattard and Bernard Evans for their thoughtful comments and careful reviews that improved the presentation and also provided critical clarification in our attempts to understand this occurrence. Manuel Iturralde-Vinent, Antonio García-Casco and Jim Pindell provided lively discussions on the geodynamic signficance of the deerite occurrence.

References

Agrell, S.O., Brown, M.G. and McKie, D. (1965) Deerite, howieite and zussmanite, three new minerals from the Franciscan of the Laytonville district, Mendocino Co., California. *American Mineralogist*, **50**, 278.

Asprey, L.B. (1976) The preparation of very pure fluorine gas. *Journal of Fluorine Chemistry*, **7**, 359–361.

Bailey, S.W. (1980) Summary of recommendations of AIPEA nomenclature committee on clay minerals. *American Mineralogist*, **65**, 1–7.

Chacko, T., Cole, D.R. and Horita, J. (2001) Equilibrium oxygen, hydrogen and carbon isotope fractionation factors applicable to geologic systems. Pp. 1–61 in: *Stable Isotope Geochemistry* (J.W. Valley and D.R. Cole, editors). Reviews in Mineralogy & Geochemistry, **43**, Mineralogical Society of America and The Geochemical Society, Washington, D.C.

Chiba, H., Chacko, T., Clayton, R.N. and Goldsmith, J.R. (1989) Oxygen isotope fractionations involving diopside, forsterite, magnetite and calcite: application to geothermometry. *Geochimica et Cosmochimica Acta*, **53**, 2985–2995.

Clayton, R.N. and Mayeda, T.K. (1963) The use of bromine pentafluoride in the exctraction of oxygen from oxides and silicates for isotope analysis. *Geochimica et Cosmochimica Acta*, **27**, 43–52.

Clayton, R.N., Goldsmith, J.R. and Mayeda, T.K. (1989) Oxygen isotope fractionation in quartz, albite, anorthite and calcite. *Geochimica et Cosmochimica Acta*, **53**, 725–733.

Coleman, R.G. and Lee, D.E. (1963) Glaucophane-bearing metamorphic rock types of the Cazadero area, California. *Journal of Petrology*, **4**, 260–301.

Deer, W.A., Howie, R.A. and Zussman, J. (1997) *Rock-forming Minerals. Volume 2B (Second Edition), Double-Chain Silicates*. The Geological Society, London, 764 pp.

Dudek, K. and Kienast, J.R. (1987) Deerite from Ile de Groix, Brittany, France. *Mineralogical Magazine*, **53**, 603–612.

Evans, B.W. and Owen, C. (2002) Phase relations of riebeckite-arfvedsonite solid solutions. *Geological Society of America Abstracts with Program*, Paper 220-5.

Fiorentini, E., Hoernes, S., Hoffbauer, R. and Vitanage, P.W. (1990) Nature and scale of fluid-rock exchange in granulite grade rocks of Sri Lanka: a stable isotope study. Pp. 311–338 in: *Granulites and Crustal*

Evolution (D. Vielzeuf and P. Vidal, editors). NATO ASI-Series, C, **311**.

Fleet, M.E. (1977) The crystal structure of deerite. *American Mineralogist*, **62**, 990–998.

Giunta, G., Beccaluva, L., Coltorti, M. and Siena, F. (2002) Tectono-magmatic significance of the peri-Caribbean ophiolitic units and geodynamic implications. Pp. 15–34 in: *Caribbean Geology into the Third Millennium: Transactions of the fifteenth Caribbean Geological Conference* (T.A. Jackson, editor). University of the West Indies Press, Mona, Jamaica.

Grafe, F. (2001) *Geochronologie metamorpher Komplexe am Beispiel der kretazischen Inselbogen-Kontinent-Kollisionszone Zentralkubas*. Unpublished Dr. rer. nat. Thesis, Ruhr-Universität Bochum, Germany.

Grevel, C. (2000) *Druck- und Temperaturentwicklung der metamorphen Deckeneinheiten des Escambray Massives, Kuba*. Unpublished Dr. rer. nat. Thesis, Ruhr-Universität Bochum, Germany.

Hatten, C.W., Somin, M., Millán, G., Renne, P., Kistler, R.W. and Mattinson, J.M. (1988) Tectonostratigraphic units of Central Cuba. *Transactions of the 11th Caribbean Geological Conference, Barbados*, 35:1–35:13.

Hollister, L.S. (1966) Garnet zoning: an interpretation based on the Rayleigh fractionation model. *Science*, **154**, 1647–1651.

Iturralde-Vinent, M.A. (1994) Cuban geology: A new plate-tectonic synthesis. *Journal of Petrology and Geology*, **17**, 1, 39–70.

Johannes, W. and Schreyer, W. (1981) Experimental introduction of CO_2 and H_2O into Mg-cordierite. *American Journal of Science*, **281**, 299–317.

Kerr, A.C., Iturralde-Vinent, M.A., Saunders, A.D., Babbs, T.L. and Tarney, J. (1999) A new plate tectonic model of the Caribbean: Implications from a geochemical reconnaissance of Cuban Mesozoic volcanic rocks. *Geological Society of America Bulletin*, **111**, 1581–1599.

Kienast, J.R. (1983) *Le métamorphisme de haute pression et de basse température (éclogites et schistes bleus): données nouvelles sur la pétrologie des roches de la croute océanique subductée et des sédiments associés*. Thèse d'état, Université P. et M. Curie, Paris.

Klein-Helmkamp, U. (1996) *Metamorphose und Exhumierung der niedrigtemperierten Hochdruckmetamorphite der Styra-Ochi-Einheit in Süd-Euböa, Attisch-Kykladisches Kristallin, Griechenland*. Dr. rer. nat. Thesis, Ruhr-Universität Bochum, Germany, 121 pp.

Lacroix, A. (1941) Les glaucophanites de la Nouvelle-Calédonie et les roches qui les accompagnent, leur composition et leur genèse. *Academie Sciences de Paris, Memoires*, **65**, 71.

Langer, K., Lattard, D. and Schreyer, W. (1977) Synthesis and stability of deerite $Fe^{2+}_{12}Fe^{3+}_{6}[Si_{12}O_{40}](OH)_{10}$, and $Fe^{3+} = Al^{3+}$ substitution at 15-28 kbar. *Contributions to Mineralogy and Petrology*, **60**, 271–297.

Lattard, D. and Le Breton, N. (1994) The *P-T-*f_{O_2} stability of deerite, $Fe^{2+}{}_{12}Fe^{3+}{}_{6}Si_{12}O_{40}(OH)_{10}$. *Contributions to Mineralogy and Petrology*, **115**, 474–487.

Leake, B.E., Woolley, A.R., Arps, C.E.P., Birch, W.D., Gilbert, M.C., Grice, J.D., Hawthorne, F.C., Kato, A., Kisch, H.J., Krivovichev, V.G., Linthout, K., Laird, J., Mandarino, J., Maresch, W.V., Nickel, E.H., Rock, N.M., Schumacher, J.C., Smith, D.C., Stephenson, N.C.N., Ungaretti, L., Whittaker, E.J.W. and Youzhi, G. (1997) Nomenclature of amphiboles: Report of the subcommittee on amphiboles of the International Mineralogical Association Commission on New Minerals and Mineral Names. *European Journal of Mineralogy*, **9**, 623–651.

Leake, B.E., Woolley, A.R., Birch, W.D., Burke, E.A.J., Ferraris, G., Grice, J.D., Hawthorne, F.C., Kisch, H.J., Krivovichev, V.G., Schumacher, J.C., Stephenson, N.C.N. and Whittaker, E.J.W. (2004) Nomenclature of amphiboles: additions and revisions to the International Mineralogical Association's amphibole nomenclature. *Mineralogical Magazine*, **68**, 209–215.

Liebau, F. (1985) *Structural Chemistry of Silicates*. Springer-Verlag, Berlin, 347 pp.

Massonne, H.-J. and Schreyer, W. (1987) Phengite geobarometry based on the limiting assemblage with K-feldspar, phlogopite and quartz. *Contributions to Mineralogy and Petrology*, **96**, 212–224.

Meschede, M. and Frisch, W. (1998) A plate-tectonic model for the Mesozoic and Cenozoic history of the Caribbean Plate. *Tectonophysics*, **296**, 269–291.

Millán, G. and Somin, M.L. (1985*a*) *Condiciones geológicas de la constitución de la capa granito-metamórfica de la corteza terrestre de Cuba*. Instituto de Geología y Paleontología, Academia de Ciencias de Cuba, La Habana, p. 83.

Millán, G. and Somin, M.L. (1985*b*) *Contribución al conocimiento geológico de las metamorfitas del Escambray y del Purial*. Instituto de Geología y Paleontología, Academia de Ciencias de Cuba, La Habana, 74 pp.

Millán-Trujillo, G. (1997) Geología del macizo metamórfico del Escambray. Pp. 271–288 in: *Estudios sobre Geología de Cuba* (G.F. Furrazola Bermúdez and K.E. Núñez Cambra, editors). Centro Nacional de Información Geológica, La Habana, Cuba.

Miyashiro, A. (1957) The chemistry, optics and genesis of alkali amphiboles. *Journal of the Faculty of*

Science, University of Tokyo, **11**, 57–83.

Muir Wood, R. (1979) The iron-rich blueschist facies minerals: I. Deerite. *Mineralogical Magazine*, **43**, 251–259.

Okay, A.I. (1980) Sodic amphiboles as oxygen fugacity indicators in metamorphism. *Journal of Geology*, **88**, 225–232.

Okay, A.I. (1987) The oxygen fugacity stability of deerite: an alternative view. *Journal of Metamorphic Geology*, **5**, 553–555.

Owen, C. (1988) *The petrogenesis of blueschist facies ironstones in the Shuksan and Easton schists, North Cascades, Washington*. Unpublished PhD thesis, University of Washington, 290 pp.

Pindell, J.L. and Barrett, S.F. (1990) Geological evolution of the Caribbean region; a plate-tectonic perspective. Pp. 405–432 in: *The Caribbean region: Boulder, Colorado* (J.E. Case and G. Dengo, editors). Geological Society of America, Boulder, Colorado; Bd. vol. H. The Geology of North America.

Pindell, J., Kennan, L., Maresch, W.V., Stanek, K.-P., Draper, G. and Higgs, R. (2005) Plate-kinematics and crustal dynamics of circum-Caribbean arc-continent interactions: tectonic controls on basin development in Proto-Caribbean margins. Pp. 7–52 in: *Caribbean/South American Plate Interactions, Venezuela* (H.G. Avé Lallemant and V.B. Sisson, editors). Geological Society of America Special Paper, **394**.

Pouchou, J.L. and Pichoir, F. (1984) Un nouveau modèle de calcul pour la microanalyse quantitative par spectrométrie de rayons X. *Recherches Aérospatiale*, **3**, 167–192.

Ramdohr, P. (1980) *The Ore Minerals and their Intergrowths*. Pergamon Press, Oxford, UK, 1205 pp.

Reinecke, T. (1987) Manganoan deerite and calderitic garnet from high-pressure metamorphic Fe-Mn-rich quartzites on Andros Island, Greece. *Mineralogical Magazine*, **51**, 247–251.

Schliestedt, M. (1980) *Phasengleichgewichte in Hochdruckgesteinen von Sifnos, Griechenland.* Unpublished Dr. rer. nat. Thesis, University of Braunschweig, Germany, 143 pp.

Schneider, J., Bosch, D., Monie, P., Guillot, A., García-Casco, A., Lardeaux, J.M., Luís Torres-Roldán, R. and Millán Trujillo, G. (2004) Origin and evolution of the Escambray Massif (Central Cuba): an example of HP/LT rocks exhumed during intraoceanic subduction. *Journal of Metamorphic Geology*, **22**, 227–247.

Somin, M.L. and Millán, G. (1974) *Geologija metamorficheskich kompleksov Kuby*. Isdat. Nauka, Moscow, 219 pp.

Somin, M.L. and Millán, G. (1981) Nekotorye tschorty struktury mezozoiskich metamorfitscheskich tol'sch Kuby. *Geotektonika*, **5**, 19–30.

Stanek, K.P. (2000) *Geotektonische Entwicklung der nordwestlichen Karibik Abriß der Geologie von Kuba*. Freiberger Forschungsheft C476, Freiberg, Germany 169 pp.

Stanek, K.P., Cobiella, J., Maresch, W.V., Millán, G., Grafe, F. and Grevel, C. (2000) Geological development of Cuba. Pp. 259–266 in: *Geoscientific Cooperation with Latin America* (H. Miller and F. Hervé, editors). *Zeitschrift für angewandte Geologie*.

Stanek, K.-P., Maresch, W.V., Grafe, F., Grevel, C. and Millán, G. (2002) Tectonics, petrology and geochronology of the Escambray complex, Central Cuba. *Caribbean Geological Conference, Barbados*, Abstract 18.

Stanek, K.-P., Maresch, W.V., Grafe, F., Grevel, C. and Baumann, A. (2006) Structure, tectonics and metamorphic development of the Sancti Spiritus Dome, eastern Escambray, Central Cuba. *Geológica Acta*, **4**, 151–170.

Stanik, E., Mañour, J. and Ching, R. (editors) (1981) *Levantamiento Escambray I. Informe de los levantamientos geológicos, geoquímicos y trabajos geofísicos, realizados en la parte sur de Cuba central en las provincias Cienfuegos, Santi Spiritus y Villa Clara*. Oficina Nacional de Minerales, Centro del Fondo Geológico Nacional, La Habana (unpublished).

Ungethüm, H. (1965) Eine neue Methode zur Bestimmung von Eisen(II) in Gesteinen und Mineralen, insbesondere auch in bitumenhaltigen Proben. *Zeitschrift für angewandte Geologie*, **11**, 500–505.

Valley, J.W. (2001) Stable isotope thermometry at high temperatures. Pp. 365–413 in: *Stable Isotope Geochemistry* (J.W. Valley and D.R. Cole, editors). Reviews in Mineralogy & Geochemistry, **43**. Mineralogical Society of America and The Geochemical Society, Washington, D.C.

Vernié, P., Kienast, J.R. and Mével, C. (1986) The occurrence of deerite in highly oxidizing conditions within the 'schistes lustrés' of eastern Corsica. *Journal of Metamorphic Geology*, **4**, 385–399.

Worthing, M.A. (1987) Deerite from Papua, New Guinea. *Mineralogical Magazine*, **51**, 689–694.

Yardley, B.W.D., Rochelle, C.A., Barnicoat, A.C. and Lloyd, G.E. (1991) Oscillatory zoning in metamorphic minerals: an indicator of infiltration metasomatism. *Mineralogical Magazine*, **55**, 357–365.

[*Manuscript received 7 July 2005: revised 10 October 2006*]